Small Antenna with Stable Impedance and Circular Polarization

Soheyl Soodmand[1], Mark A. Beach[1], Kevin A. Morris[1]
[1]dept. electrical and electronic engineering, university of Bristol, Bristol, United Kingdom, soheyl.soodmand@bristol.ac.uk

***Abstract*—Variations in antenna impedance with respect to frequency significantly reduces the isolation bandwidth in some modern 5G communication systems like In-Band Full Duplex (IBFD) transceivers. A frequency independent antenna with a core structure of equiangular Archimedean spiral is designed to achieve impedance stability in frequency domain. The antenna impedance at an ultra-wideband (UWB) frequency range of 1.5GHz to 4GHz is more smoothened in some design steps to achieve an stable impedance using electromagnetic absorbers, capacitive impedance tuning and modification techniques whilst this small antenna also has circular polarization, electromagnetic compatibility, and suitable radiation efficiency.**

***Index Terms*—antennas, in-band full duplex, 5G, frequency independent antenna, stable impedance, circular polarization.**

I. INTRODUCTION

Future communication systems, such as 5G and 6G, will be required to support numerous radio access over a wide range of frequencies. In-band full-duplex (IBFD) systems can theoretically double link capacity of Time Division Duplex (TDD) and Frequency Division Duplex (FDD) systems thus allowing simultaneous transmission and reception on the same frequency and reduce latency [1], [2]. Transmitting and receiving on the same time-frequency resource results in strong co-channel Self-Interference (SI) which will effectively increase the receiver noise floor, reducing the capacity of the receive channel [3].

Recent results [3]–[5] have demonstrated that Electrical Balance Duplexer (EBD) in IBFD transceivers, Fig. 1, implements a form of SI cancellation (SIC) in order to provide high transmit (TX) to receive (RX) isolation. The analog technique of EBD is achieved by coupling transmitter, receiver and antenna using a four-port hybrid junction, along with a balancing impedance connected to the fourth port. High TX-RX isolation is expected when the balancing impedance is equal to the antenna impedance at all frequencies within that band. However, in practice, the antenna impedance is not an ideal 50 Ω resistor but has a complex impedance which exhibits variations with respect to frequency in resistive and reactive parts so the isolation will be limited by the impedance mismatching between the antenna and balancing impedance. Measured real antenna data in [3], [6] for a prototype EDB demonstrate that the variation in antenna impedance significantly reduces the SIC bandwidth, and is the dominant factor in limiting the TX-RX isolation.

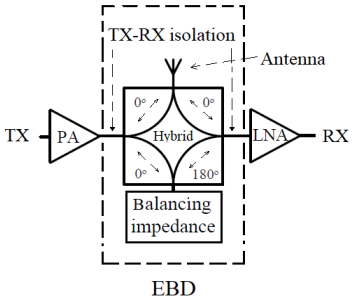

Fig. 1. Electrical Balance Duplexer in In-Band Full-Duplex system

The main aim in this work is to design an antenna with high impedance stability in frequency domain for systems like mentioned above. In Section II, a summary on frequency independent spiral antennas is given. Spiral Archimedean antenna with copper case is investigated in Section III as a core structure to start design of an antenna with high impedance stability. Then, the impedance variations of the antenna are reduced in Section IV by adding two rings made up of electromagnetic absorber to the core structure of Section III. In Section V, more improvement in impedance stability is achieved by employing capacitive impedance tuning and some modification. Finally, a conclusion is given in Section VI.

II. FROM FREQUENCY INDEPENDENT ANTENNAS TOWARDS SPIRAL ANTENNAS

In practice, antenna shapes exist that completely specified by angles to have frequency independent characteristics in impedance, pattern, polarization, and so forth, and with current distribution which diminishes rapidly [7]. The analytical treatment of frequency independent antennas is presented in [7]–[9]**.** Classical shapes of frequency independent antennas include the equiangular geometries of planar and conical spiral structures[10], [11], and the logarithmically periodic structures [12].

In the equiangular spiral since a curve along its surface extends to infinity, it is necessary to designate the length of the arm to specify a finite size antenna. The lowest frequency of operation for a spiral antenna occurs when the total arm length is comparable to the wavelength [10]. For all frequencies above this, the pattern and impedance characteristics are almost frequency independent. Initial analytical formulations are given in [8] to describe single arm, two arm and multiple arm spirals (where arms are

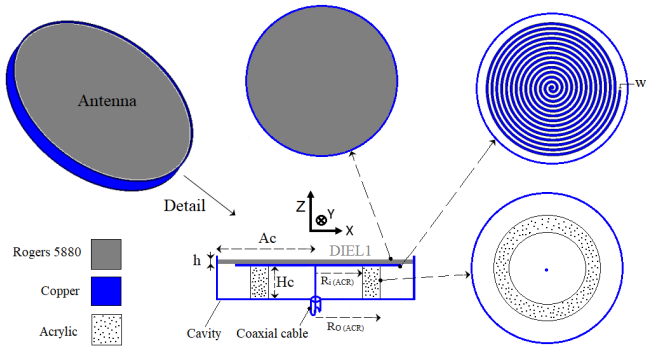

Fig.2. Archimedean spiral antenna described in Section III (whole and cross-section views).

metallic), and the other of a spiralling slot on a large conducting plane while all these antennas are considered to be suspended in free space.

There have been also basic investigations of the radiation characteristics of spiral antennas with metallic arms [13], [14]. Investigations in [13] have been made under the condition that the spiral antennas have two arms (in free space without a conducting plane reflector). Beam investigation for the case of a multi-arm spiral antenna is given in [14]. The feed systems for two- and multi-arm spiral antennas are complicated because a balun or an excitation circuit consisting of power dividers and phase shifters is required for practical use. Single-arm spiral antenna which has a simpler arm configuration and a simpler feed system than two- and multi-arm spirals is analyzed [15] in the presence of an infinite conducting plane reflector (a ground plane). In the rest of this paper a monofilar single arm antenna with a cylindrical copper case is considered as a core structure to design an antenna with high impedance stability, in frequency domain.

III. Archimedean Spiral Antenna with Copper Case

A single arm Archimedean Spiral (AS) is backed by a cavity in this section, Fig. 2, to have a unidirectional beam and to reduce Electromagnetic interference (EMI) to be used in a potential compact wireless module. The AS is formed as a single conducting spiral strip arm of width w on bottom of a disc shaped Rogers RT 5880 substrate of radius A_C = 62 mm with a dielectric constant of ε_r = 2.2, loss tangent of 0.0009, h=0.79-mm thickness plus a 9 μm-thick copper coating. This dielectric substrate, so called DIEL1, has no copper on the top. The centerline of the spiral arm is defined by the Archimedean function of r = K Φ, where K is the spiral constant and Φ is the winding angle, ranging from starting angle Φ_S to ending angle Φ_E. The antenna circumference C is defined by C = 2π R_{max} with R_{max} = K Φ_E. The AS is defined using the following configuration parameters: K = 0.64 mm/rad, Φ_S = 0.07π Rad , Φ_E = 28π Rad, R_{max}= 56 mm and w = 2mm knowing that the lowest frequency of operation occurs when the total arm length is comparable to the wavelength.

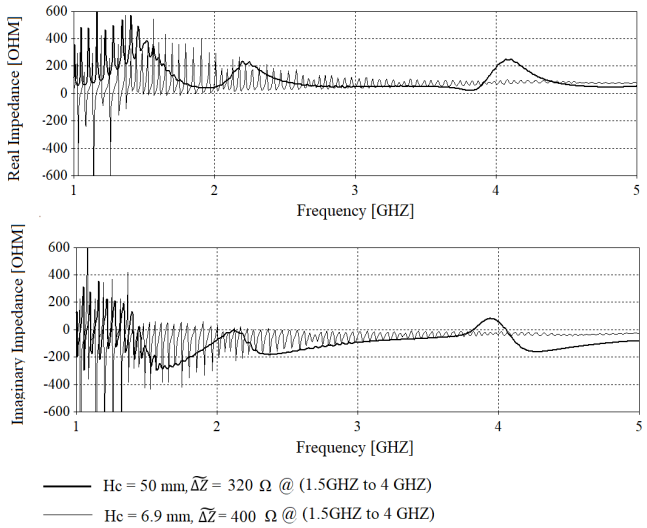

Fig. 3. Impedance and $\widetilde{\Delta Z}$ of antenna in Fig.2 when H_C = 50 mm = 0.25 λ_L and H_C = 6.9 mm = 0.035 λ_L.

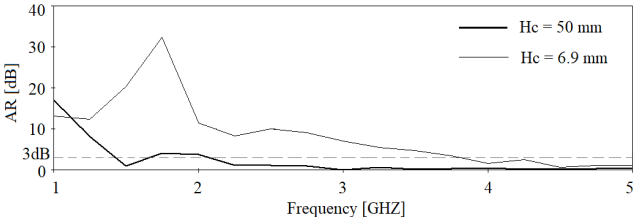

Fig. 4. Axial ratio versus frequency plot of antenna in Fig.2 when H_C = 50 mm = 0.25 λ_L and H_C = 6.9 mm = 0.035 λ_L.

The cavity radius, A_C, has 6 mm distance from the arm end to the cavity wall as A_C = 62 mm= 0.31 λ_L whilst λ_L is the wavelength at the lowest design frequency of 1.5 GHz. The spiral is fed by a 50 Ω coaxial cable whereas the inner conductor of the cable is connected to the AS at its starting angle and outer ground conductor of the cable is connected to the bottom of copper case at the centre. The distance between the bottom of the cavity and the spiral on the bottom of DIEL1 substrate is shown by H_C. To hold the DIEL1 substrate a cylindrical ring is 3D printed on Acrylic material with a dielectric constant of $\varepsilon_{r(ACR)}$ = 3.5, internal radius of $R_{i(ACR)}$ = of 41 mm, outer radius of $R_{O(ACR)}$ = 51 mm and the same height with H_C. There is not a noticeable difference in results for antenna with and without Acrylic ring holder, so the results in this paper are given for structure with Acrylic ring only for briefing. The height of the copper case wall is chosen as H_C + 2h to surround the DIEL1 disc substrate while the case has a 1 mm uniform thickness of copper. The antenna structure with details is shown in Fig.2.

Analysis

The Finite Integration Technique (FIT) with high meshing in CST MICROWAVE STUDIO [16] software is used to obtain input impedance data plot of the antenna for a

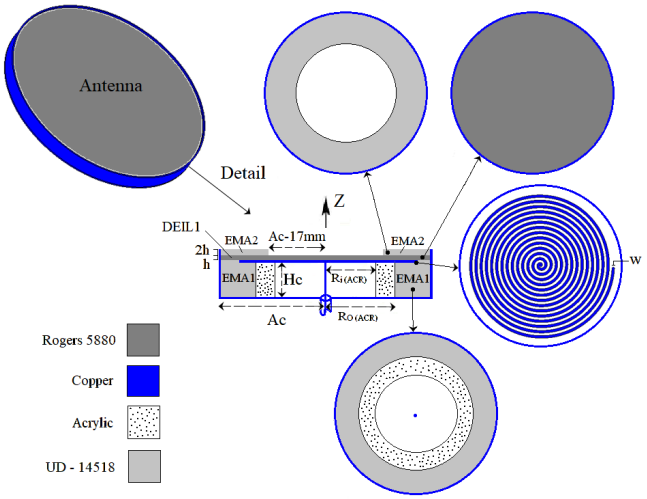

Fig. 5. Archimedean spiral antenna with EMAs described in Section IV (whole and cross-section views).

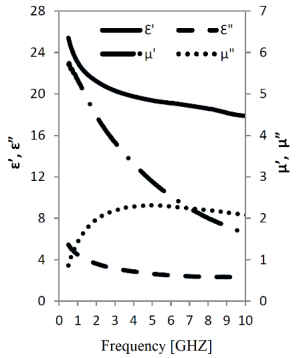

Fig. 6. Permittivity and permeability characteristics of UD-14518 EMA from [19].

quarter of wavelength distance of H_C = 50 mm =0.25 λ_L as results are shown in Fig. 3. However, the purpose here is to construct a compact efficient antenna with stable impedance and working on an antenna with the height of H_C = 50 mm goes against this purpose.

For H_C < 6.9 mm the antenna impedance plot (not shown here) goes to very high out of the order variations even more than the variations seen in the Fig.3. To realize an electrically small antenna H_C = 6.9 mm = 0.035 λ_L is chosen but the simulated input impedance does not exhibit a suitable impedance stability yet and noticeable dense variations specifically are seen at lower frequencies, Fig.3. These dense impedance variations are due to the reflection of electromagnetic waves at the bottom of the copper case; as the frequency is decreased, the electrical antenna height decreases and the reflected electromagnetic waves which imping on the spiral become stronger. These reflected waves affect the current along the conducting spiral arms and as seen resulted into an out of order dense impedance instabilities. Average of impedance variations in the bandwidth of interest is defined as

$$\widetilde{\Delta Z} = \frac{|\Delta\, Real(Z)| + |\Delta Imag(Z)|}{2} \qquad (1)$$

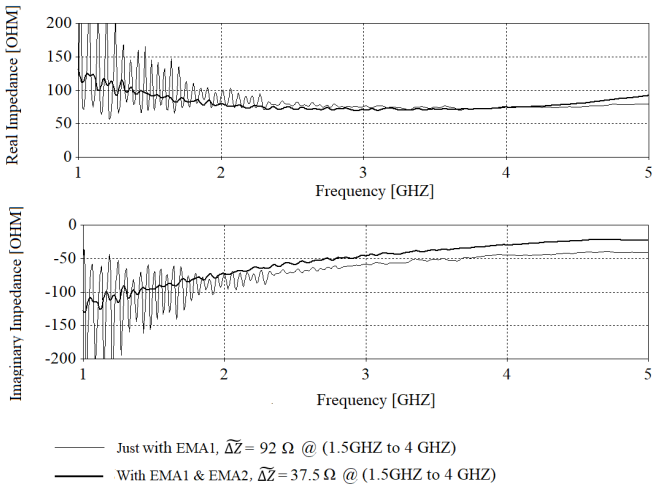

Fig 7. Impedance and $\widetilde{\Delta Z}$ of antenna in Fig.5 (with EMAs and H_C = 6.9 mm).

where Δ *Real* (*Z*) is maximum variation (Max. impedance - Min. impedance) of real impedance and Δ *Imag* (*Z*) is maximum variation of imaginary impedance in the bandwidth of interest. For antenna with copper case in this section $\widetilde{\Delta Z}$ = 320 Ω is calculated when H_C=50 mm and $\widetilde{\Delta Z}$ = 400 Ω is calculated for H_C=6.9mm at 1.5GHz to 4GHz range.

The change in the current distribution caused by the decrement in H_C affects not only the impedance, but also the Axial Ratio (AR). To have an antenna with circular polarization AR < 3dB is needed and as shown in Fig. 4 the simulated AR deteriorates for H_C = 6.9 mm in comparison with H_C = 50 mm. Improvements in the impedance stability and AR for the antenna with H_C=6.9 mm is discussed in Sections IV and V.

IV. Lowering Impedance Variation by Two Ring Shape Electromagnetic Absorbers

In the antenna with H_C = 6.9mm of copper case in Section III, the remaining current along the outermost arms, source of the electromagnetic (EM) fields reflected at the bottom of the copper case, causes dense variations in the input impedance specifically at low frequencies, Fig. 3. It is necessary to attenuate this reflected fields for the antenna to make the impedance more stable in UWB frequency range using techniques as employing lossy material [17], [18]. As shown in Fig. 5, a ring-shaped EM Absorber (EMA) strip - so called EMA1- of width 11mm = A_C - $R_{O(ACR)}$ and with the same height of copper case H_c = 6.9 mm is placed under the antenna arms to fill the space between the cavity wall and Acrylic holder ring. The EMA1 is a nonconducting dielectric material and specified by complex relative permittivity $\varepsilon_r=\varepsilon'$-j$\varepsilon''$ and complex relative permeability $\mu_r=\mu'$-jμ''. Optimization of ε_r to smooth the input impedance frequency response is performed using different commercially available EMAs and the smoothest impedance response is obtained when using model UD-14518 of ARC

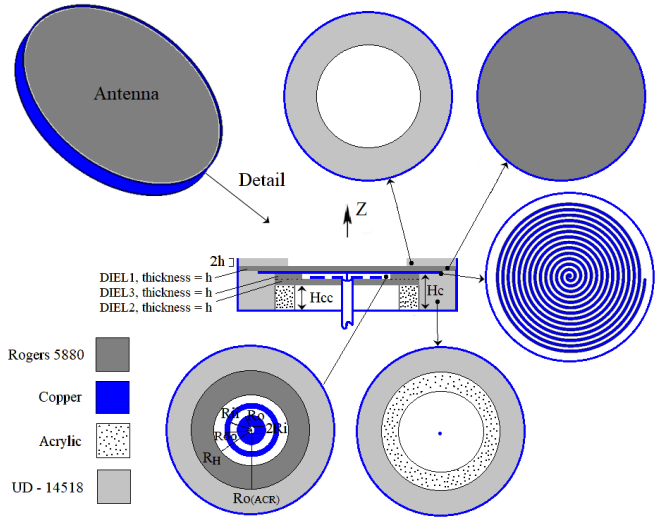

Fig. 8. Final antenna: Archimedean spiral antenna with EMAs and capacitive tuning, described in Section V (whole and cross-section views), dimensions of common elements are the same with antenna in Fig.5 just Acrylic height is shortened from H_C to H_{CC} to place DIEL2 and DIEL3.

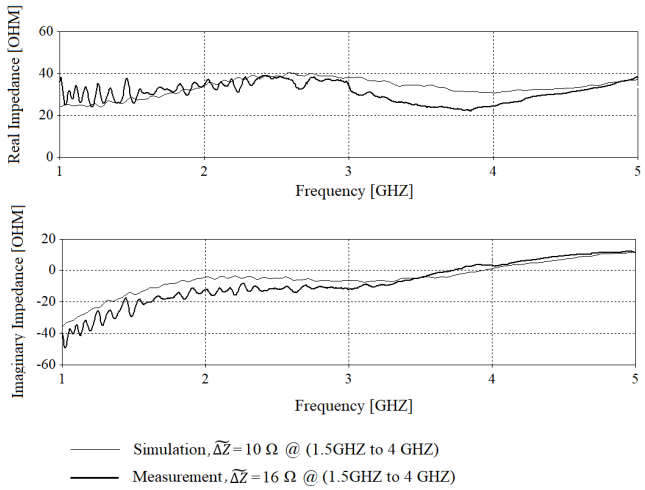

Fig. 9. Measured/Simulated Impedance and $\widetilde{\Delta Z}$ of final antenna.

Technology Ltd whose permittivity and permeability plots from [19] are given in Fig.6.

Fig. 7 shows the input impedance as a function of frequency in simulation, where the results are obtained using the parameters of the ARC UD-14518 absorber as constituent material of EMA1. Width of EMA1 is optimized to be 11 mm at the lower operating design frequency of 1.5 GHz considering impedance stability. It is found that the deterioration in impedance stability at low frequencies, observed for the antenna having H_C =6.9 mm Section III, is improved with the EMA1, Fig.7. Consequently, the spiral exhibits smoother wideband impedance characteristics ($\widetilde{\Delta Z}$ = 92 Ω at 1.5GHz to 4GHz range) much lower than for the antenna without EMA1 ring in Section III.

Also, by adding a second EMA, so called EMA2, made up of the same UD-14518 material to above the DIEL1 substrate (Fig. 5) better impedance stability is obtained, Fig.

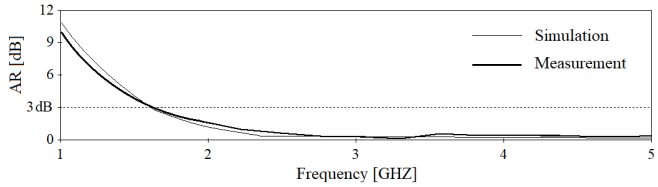

Fig. 10. Simulated and measured AR versus frequency plot of final antenna.

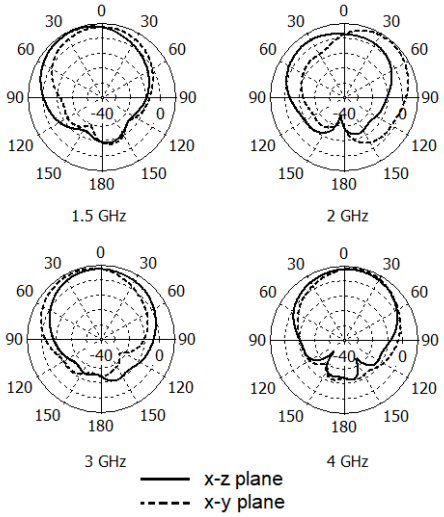

Fig. 11. Measured directivity pattern of final antenna.

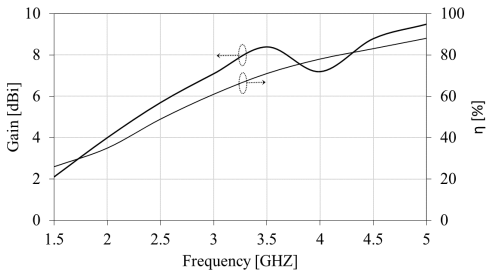

Fig. 12. Measured gain and radiation efficiency of final antenna.

7, with $\widetilde{\Delta Z}$ = 37.5 Ω at 1.5GHz to 4GHz range. EMA2 has an optimized thickness of 2h = 1.6 mm while its outer radius is equal to the cavity diameter of A_C and its inner radius is A_C - 17mm = 45mm.

V. Final Antenna, More Improvement in Impedance Stability by Capacitive Impedance Tuning and Spiral Modification

As seen in Fig. 7, the antenna with EMAs in Section IV has higher impedance instability in its inductive impedance than its resistive impedance whilst also it has a high resistive impedance value which necessitate using balun to match it to a standard 50 Ω feed. A capacitive impedance matching solution using two cocentric planar copper rings is suggested in this section, Fig. 8, to mitigate inductive impedance instability, and to decrease and smoothen the resistive

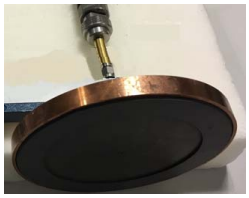

Fig. 13. Fabricated antenna.

impedance of the antenna without using any balun. Maximum bandwidth for higher impedance stability in 1.5 GHz to 4 GHz range is achieved when a material with low dielectric constant of ε_r =1 is considered between the copper rings and the spiral to form a capacitive impedance tuning therefore air with ε_r =1 is chosen as the most suitable material.

As seen in Fig.8, the two cocentric planar copper rings are considered on the top surface of a disc shape dielectric material, so called DIEL2, while there is a distance of h = 0.79 mm between the copper rings and the spiral body. DIEL2 with a thickness of h is made up of the same material of Rogers RT 5880, which is used before for DEIL1. DIEL2 has a small hole with R_i = 1.7mm radius in the centre for passing the coaxial cable whilst the outer radius of DIEL2 is equal to the inner radius of Acrylic holder, $R_{i\ (ACR)}$ = 41mm. Also, a planar dielectric ring, so called DIEL3, with the same thickness and the same material with DIEL2 is used as a spacer between DIEL2 and DIEL1 to provide a suitable area for air. DIEL3 has a hole with radius of R_H = 35mm in the centre, Fig.8, whilst its outer radius is equal with the outer radius of DIEL2. The height of Acrylic ring, which was 6.9mm in the previous sections, is reduced to $H_{CC} = H_C - 2h$ = 5.3mm, Fig.8, to provide a place for DIEL2 and DIEL3 substrates without changing the whole antenna height. This height change in the Acrylic ring does not show any noticeable destroying impact on the impedance stability and radiation performance. The internal copper ring has an optimized inner radius of R_i=1.7mm and outer radius of R_O= 5.5 mm while the external ring has inner radius of R_{ii} = 7.5 mm and outer radius of R_{OO} =10.5 mm, Fig. 8. The coaxial cable is also extended from the bottom of case to the top surface of DIEL3 substrate where the cable outer conductor (ground) is connected to the inner radius of internal capacitive ring.

However, an optimum impedance stability with of $\widetilde{\Delta Z}$= 10 Ω is obtained from the simulated impedances for final antenna whilst $\widetilde{\Delta Z}$= 16 Ω is calculated from the measured impedance data, all given in Fig. 9 at 1.5GHz to 4GHz range. This shows significant improvements in impedance instability in comparison with the antennas in Section III and IV. Measured and simulated AR for the final antenna are given in Fig.10 indicating a circular polarization of AR < 3dB over 1.6 GHz. Also, measured directivity pattern and measured gain/efficiency are shown respectively in Fig. 11 and Fig. 12, all indicating suitable impedance stability and radiation performance at 1.5 GHz to 4 GHz range. Fabricated antenna is shown in Fig. 13.

VI. Conclusion

Variations in antenna impedance with respect to frequency is the dominant factor to significantly reduce isolation bandwidth and value in some modern communication systems like IBFD transceivers.A frequency independent antenna having Archimedean spiral core is designed to achieve high impedance stability at an ultra-wideband (UWB) frequency range of 1.5GHz to 4GHz. Antenna design was carried in some steps using electromagnetic absorbers, capacitive impedance tuning and modification techniques to smooth the impedance whilst small antenna dimension, circular polarization, electromagnetic compatibility, and suitable radiation efficiency were obtained for the designed antenna.

References

[1] L. Laughlin *et al.*, "Tunable Frequency-Division Duplex RF Front End Using Electrical Balance and Active Cancellation," *IEEE Trans. Microw. Theory Tech.*, vol. 66, no. 12, pp. 5812–5824, 2018.

[2] A. Sabharwal, P. Schniter, D. Guo, D. W. Bliss, S. Rangarajan, and R. Wichman, "In-band full-duplex wireless: Challenges and opportunities," *IEEE J. Sel. Areas Commun.*, vol. 32, no. 9, pp. 1637–1652, 2014.

[3] L. Laughlin, M. A. Beach, K. A. Morris, and J. L. Haine, "Optimum single antenna full duplex using hybrid junctions," *IEEE J. Sel. Areas Commun.*, vol. 32, no. 9, pp. 1653–1661, 2014.

[4] M. Mikhemar, H. Darabi, and A. A. Abidi, "A multiband RF antenna duplexer on CMOS: Design and performance," *IEEE J. Solid-State Circuits*, vol. 48, no. 9, pp. 2067–2077, 2013.

[5] L. Laughlin, M. A. Beach, K. A. Morris, and J. L. Haine, "Electrical balance duplexing for small form factor realization of in-band full duplex," *IEEE Commun. Mag.*, vol. 53, no. 5, pp. 102–110, 2015.

[6] B. Debaillie *et al.*, "Analog/RF solutions enabling compact full-duplex radios," *IEEE J. Sel. Areas Commun.*, vol. 32, no. 9, pp. 1662–1673, 2014.

[7] V. Rumsey, "Frequency independent antennas," in *1957 IRE National Convention Record*, 1957, pp. 114–118.

[8] C. A. Balanis, *Antenna Theory: Analysis and Design*, 3rd ed. Wiley–Blackwell, 2005.

[9] R. S. Elliott, "A View of Frequency Independent Antennas," *Microw. J.*, vol. 5, pp. 61–68, 1962.

[10] J. D. Dyson, "The Equiangular Spiral Antenna," *IRE Trans. Antennas Propag.*, vol. AP-7, no. 2, pp. 181–187, 1959.

[11] D. S. Filipović and J. L. Volakis, "Novel slot spiral antenna designs for dual-band/multiband operation," *IEEE Trans. Antennas Propag.*, vol. 51, no. 3, pp. 430–440, 2003.

[12] D. E. Isbell, "Log Periodic Dipole Arrays," *IRE Trans. Antennas Propagat*, vol. AP-8, pp. 260–267, 1960.

[13] R. T. Gloutak and N. G. Alexopoulos, "On the theory of eccentric spiral antennas," in *IEEE Ant. and Prop. Soci. AP-S Inte. Symp.*, 1992, vol. 1992-June, pp. 2097–2100.

[14] L. Shafai, "Design of multi-arm multi-mode spiral antennas for directional beams using equivalent array concept," *Electromagnetics*, vol. 14, no. 3–4, pp. 285–304, 1994.

[15] H. Nakano, "A monofilar spiral antenna and its array above a ground plane-formation of a circularly polarized tilted fan beam," *IEEE Trans. Antennas Propag.*, vol. 45, no. 10, pp. 1506–1511, 1997.

[16] "CST Studio Suite Electromagnetic Field Simulation Software (2020)." DASSAULT SYSTÈMES, [Online]. Available: https://www.3ds.com/products-services/simulia/products/cst-studio-suite/.

[17] J. J. H. Wang and V. K. Tripp, "Design of Multioctave Spiral-Mode Microstrip Antennas," *IEEE Trans. Antennas Propag.*, vol. 39, no. 3, pp. 332–335, 1991.

[18] S. Lipsky, *Microwave Passive Direction Finding*. New York: Wiley-Interscience, 1987.

[19] "[Online]. Available." https://www.hitek-ltd.co.uk/index.php/downloads/dl/file/id/9822/product/0/ud_14518_rev_b_8ghz_urethane_1_14mm.pdf.